THE JOURNAL OF PHYSICAL CHEMISTRY C

Article

pubs.acs.org/JPCC

Sorption Isotherms of Water in Nanopores: Relationship Between Hydropohobicity, Adsorption Pressure, and Hysteresis

Matías H. Factorovich,[†] Estefanía Gonzalez Solveyra,[†] Valeria Molinero,[‡] and Damián A. Scherlis*,[†]

[†]Departamento de Química Inorgánica, Analítica y Química Física/INQUIMAE, Facultad de Ciencias Exactas y Naturales, Universidad de Buenos Aires, Ciudad Universitaria, Pab. II, Buenos Aires C1428EHA, Argentina

[‡]Department of Chemistry, The University of Utah, 315 South 1400 East, Salt Lake City, Utah 84112-0850, United States

Supporting Information

ABSTRACT: The motivation of this study is to elucidate how the condensation and desorption pressures in water sorption isotherms depend on the contact angle. This question is investigated for cylindrical pores of 2.8 nm diameter by means of molecular dynamics simulations in the grand canonical ensemble, in combination with the mW coarse-grained model for water. The contact angle is characterized for different sets of water–surface interactions. First, we show that desorption in open-ended pores with moderate or low water affinity, with contact angles greater or equal than 24°, is a nonactivated process in which pressure is accurately described by the Kelvin equation. Then, we explore the influence of hydrophobicity on the capillary condensation and on the width of the hysteresis loop. We find that a small increase in the contact angle may have a significant impact on the surface density and consequently on the nucleation free energy barrier. This produces a separation of the adsorption and desorption branches, exacerbating the emerging hysteresis. These results suggest that the contact angle is not as relevant as the adsorption energy in determining condensation pressure and hysteresis. Finally, we consider nonequilibrium desorption in pores with no open ends and describe how homogeneous and heterogeneous cavitation mechanisms depend on hydrophilicity.

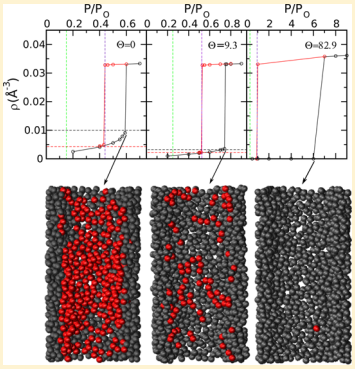

INTRODUCTION

The thermodynamics of confined fluids in the context of adsorption in porous materials has been the subject of continued research for more than seven decades. The development of the modern theoretical framework to understand the phenomena of adsorption, capillary condensation, and hysteresis in confined spaces may be tracked to the 1940s, with the contributions of many authors including Cohan, Emmett, Katz, Everett, Derjaguin, and Prigogine, among others.[1−7] The fluid uptake by a porous matrix is characterized by the adsorption–desorption isotherm, which measures the amount of substance adsorbed in the material as a function of the relative vapor pressure. These isotherms typically exhibit a surface adsorption plateau at low pressures, followed by the capillary condensation branch—where the content of adsorbed fluid jumps abruptly—and a final high pressure plateau corresponding to the material mostly filled with a condensed phase.[8,9] In pores above a certain size, typically 2 nm diameter, adsorption–desorption hysteresis is observed.[10] For a given adsorbate, there is a critical temperature (the so-called capillary critical temperature) which depends on the pore size and on the specific adsorbate–surface interactions, above which capillary condensation is suppressed and replaced by continuous or reversible pore filling.[8,11] Capillary condensation may require surmounting a free energy barrier to nucleate the liquid from the low density, surface adsorbed phase, and therefore it arises at a pressure lying somewhere between the equilibrium point and the vapor spinodal. Desorption, on the other hand, is believed to proceed in equilibrium in straight, open-ended pores, but below the equilibrium transition pressure in more complex geometries, as in the case of pores with blocked-ends or inhomogeneous diameter, where evaporation may be hindered by different mechanisms (e.g., pore blocking or cavitation).[9] For a given substance, the detailed shape of the curves depends on temperature, hydrophilicity of the walls, pore size and connectivity, and therefore an appropriate interpretation of sorption isotherms may provide insights into all those properties.

In the case of water, the earliest measurements of sorption in uniform mesoporous materials were focused on MCM-41 silica matrices, revealing an adsorption pattern characteristic of type V isotherms, with a pronounced capillary condensation step accompanied by sorption–desorption hysteresis.[12,13] A similar behavior was reported for water in FSM-16 silica nanopores,[10] where the gap between adsorption and desorption pressures is observed to decrease with pore size and to disappear altogether for a diameter situated between 1.4 and 2.0 nm—which is larger than the critical size found for gases like nitrogen, argon, or oxygen in the proximity of their corresponding normal boiling temperatures.[14,15] In both porous materials, a significant

Received: May 24, 2014
Revised: June 25, 2014
Published: June 26, 2014

   dx.doi.org/10.1021/jp5000396 | J. Phys. Chem. C 2014, 118, 16290–16300

shift to lower condensation pressures was informed for the second sorption run and attributed to an enhancement in hydrophilicity due to hydroxylation following the first adsorption cycle.[10,16,17] Grünberg and co-workers proposed two possible filling mechanisms for water at 298 K based on NMR analysis of mesoporous silica pores with a different radius.[18] According to their results, in the narrower pores (3.3 nm diameter MCM-41) capillary condensation is preceded by monolayer coverage, whereas in the wider pores (8 nm diameter SBA-15) a radial thickening involving several layers takes place before capillary condensation occurs. A lot of effort has also been directed to understanding water in highly hydrophobic environments. Studies in porous carbons or in nanotubes of pore size in the range of a few nanometers have shown that H_2O penetrates and is retained by the hydrophobic matrix.[19−21] While the adsorbed amount is negligible at low pressures, further filling gives rise to capillary condensation at a water relative pressure usually between 0.5 and 1, depending on pore size and on the presence of active sites.

Computer simulations have played a central role in the elucidation of the filling mechanisms and phase transitions taking place during the adsorption/desorption process. A considerable amount of work has been carried out with Lennard−Jones models representing simple fluids like Ar or N_2 in cylindrical and slit pores.[22−26] For these systems, the adsorption and desorption pressures, the degree of hysteresis, the density profiles, and other properties related to the gas−liquid transition have been characterized as a function of temperature and pore size, on the basis of density functional theory[27] and molecular simulations.[28] Recent work has addressed the role of pore roughness[29] and shape.[30] While a large fraction of the computational research on the phase behavior in confinement has focused on simple adsorbents, several other more complex kinds of fluids have also been widely investigated. Hydrocarbons and carbon dioxide adsorption has been extensively studied in zeolites and in other materials relevant for energy applications.[31−33] Water, on the other hand, has been examined in silica and in hydrophobic environments by several authors. Brovchenko and collaborators[34] applied Monte Carlo simulations in the Gibbs ensemble for TIP4P water confined in featureless cylindrical and slit pores of sizes comprised between 1.2 and 2.4 nm. Many different conditions were examined from 200 to 600 K, finding liquid−vapor coexistence on a large temperature range, depending on the hydrophilicity and pore size. They observed bulk-like liquid−vapor phase transitions in hydrophobic pores, identifying three additional types of phase coexistence in more hydrophilic systems, which were classified as first layering transition, second layering transition, and prewetting. Liquid coexistence with an adsorbed bilayer was typically seen for the most hydrophilic pores.[34] In a later investigation based on Monte Carlo and molecular dynamics simulations,[35] Shirono and Daiguji explored the phase behavior of SPC/E water in silica pores in the range of 1−3 nm of diameter. Three different phases were characterized, consisting of, respectively, a submonolayer coverage with water molecules exclusively solvating the silanol groups, a condensed monolayer, and a completely water-filled pore. Siboulet and co-workers investigated the role of amorphousness in the hydrophilic to hydrophobic transition, for which they built amorphous silica pore models combining Monte Carlo with a simulated annealing technique.[36] They concluded that the amorphicity of the surface is not a determinant factor, suggesting that hydrophilicity is mostly related to charged or uncharged defects on the interface. The increase in hydrophilicity produced a significant shift of the adsorption pressure toward higher values. Such a shift induced by the modulation of the fluid−wall interaction has been proven by Schreiber, Bock, and coauthors, combining experiment and simulations for a polar adsorbent, CHF_3.[37] In recent work based on NVT molecular dynamics of mW water[38] in moderately hydrophilic pores with adsorption energies comparable to those found in MCM-41 and FSM-16 silica, we have shown that there is an onset filling at which capillary condensation is unleashed, forming a condensed liquid phase, which coexists with a low-density phase consisting of water adsorbed on the pore walls.[39] Above this water content, further addition of molecules to the system does not alter the densities of the two phases in equilibrium but causes an increase in the amount of the condensed liquid phase. Our simulations revealed two filling mechanisms for pores in the range 3.0−4.0 nm, depending on the water−surface affinity: (i) a localized growth of a water droplet for surfaces of moderate hydrophobicity, and (ii) an homogeneous filling leading to water densities above equilibrium for hydrophilic nanopores.[40] These mechanisms were also verified in later molecular dynamics simulations of SPC/E water in TiO_2 pores.[41] Computational studies of water in hydrophobic graphitic pores of various shapes, with bare surfaces or decorated with active groups, have been conducted by a number of researchers employing grand canonical Monte Carlo techniques.[42−47]

In spite of all this work to elucidate different aspects of water adsorption in nanopores, there are still central questions which remain mostly unexplored. One such question is what is the systematic role of hydrophilicity on the capillary condensation and the adsorption hysteresis in water isotherms. In the present study, we combine grand canonical molecular dynamics simulations with the mW model for water to obtain equilibrium, nonequilibrium, and dynamical information on the liquid−vapor transitions in realistic models of cylindrical pores. First, we characterize the equilibrium transition point—given by the desorption pressure—as a function of the contact angle. In particular, we find that the Kelvin equation is rigorously verified for contact angles greater or equal than 20°. Second, we explore the influence of hydrophobicity on the capillary condensation and on the width of the hysteresis loop. We show that an increase in the contact angle has a greater impact on the adsorption than on the desorption pressure, thus enhancing the resulting hysteresis. Moreover, we argue that the contact angle is less relevant than the adsorption energy in determining the condensation pressure. Even if both contact angle and adsorption energy are directly related to the free energy of the fluid-surface interaction, the relation between the two is by no means direct, nor is it straightforward to establish accurately from fundamental considerations. The adsorption energy as defined in this work is the interaction of water molecules with the cylindrical pore at zero coverage, whereas the contact angle, according to Young's equation, depends on three interfacial tensions, of which the fluid−solid contribution is also determined by the interaction of the fluid with itself. Lastly, we investigate nonequilibrium desorption and describe how homogeneous and heterogeneous cavitation mechanisms depend on hydrophilicity.

METHODOLOGY

Grand Canonical Molecular Dynamics Simulations. The grand canonical molecular dynamics approach (GCMD)

dx.doi.org/10.1021/jp5000396 | J. Phys. Chem. C 2014, 118, 16290−16300

allows for particle exchange with a reservoir, to provide a temporal description of a molecular system at a controlled chemical potential μ. The algorithm reproduces a grand-canonical ensemble where particles can be deleted or created in the simulation box.[48,49] The equations of motion for water were integrated using the velocity Verlet algorithm with a time step of 5 fs, applying the Nosé−Hoover thermostat with a relaxation time of 0.5 ps. Along the grand canonical dynamics, a number of attempts of particle insertion and deletion is realized at every time-step: this number is the so-called GC/MD ratio. It is desirable to keep this parameter as low as possible to minimize computer time, but in turn it must be high enough to ensure that the target chemical potential is reached during the simulation.[49,50] GC/MD ratios in the range 20−100 have been typically used in previous studies.[49−51] In our simulations, a GC/MD ratio of 20 was adopted, which is common in the literature and gives converged results for the systems examined here. GCMD simulations were performed using a properly modified version of the LAMMPS program.[52]

Water Force Field. The interaction between water molecules was represented with the mW coarse-grained model, in which each H_2O molecule is treated as a single particle interacting through anisotropic short-ranged potentials that encourage tetrahedrally coordinated structures.[38] The mW model uses the short-ranged interaction form of the Stillinger−Weber potential, consisting of a sum of two-body attraction terms, which favor high coordination, and three-body repulsion terms, which reinforce tetrahedral "hydrogen-bonded" configurations:

$$E = \sum_{i,j>i} A\varepsilon\left[B\left(\frac{\sigma}{r_{ij}}\right)^4 - 1\right]\exp\left(\frac{\sigma}{r_{ij} - a\sigma}\right) + \sum_{i,j\neq i,k>j} \lambda\varepsilon[\cos\theta_{ijk} - \cos\theta_0]^2 \exp\left(\frac{\gamma\sigma}{r_{ij} - a\sigma}\right) \exp\left(\frac{\gamma\sigma}{r_{ik} - a\sigma}\right) \quad (1)$$

where r_{ij} is the distance between particles i and j, θ_{ijk} is the angle defined by particles i, j, and k, A = 7.049556277, B = 0.6022245584, γ = 1.2, a = 1.8, and θ_0 = 109.47°. The value of the parameter λ = 23.15 dictates the strength of the tetrahedral interactions, while σ = 2.3925 Å and ε = 6.189 kcal/mol modulate the characteristic length and strength of water−water interactions, respectively. It is worth mentioning that although the mW model does not include electrostatic terms or explicit hydrogen atoms, it is able to accurately reproduce the phase behavior for the solid−liquid equilibria in bulk, and in confinement, it has been successfully employed to describe the anomalies and structure of solid and liquid water, and it gives a qualitatively correct description of the liquid−vapor coexistence in terms of relative pressure.[39,40,53−56] The computational cost of mW simulations is on the order of 1% compared with atomistic simulations.[38] The speedup arises from the smaller number of particles, the longer timesteps (10 versus 1.5 fs), and shorter range of interactions (cutoff at 4.32 Å versus Ewald sums).

Model of the Pore. The pore is formed by mW particles, with a structure derived from an instantaneous configuration of liquid water simulated at 298 K and 1 atm in periodic boundary conditions.[39,40] A channel of 28 Å diameter was built removing a cylindrical block of water molecules, to produce nanopores of length 77 Å with amorphous walls (see the Supporting Information for a detailed definition of the pore diameter). The walls are always wider than 1 nm, well beyond the 4.32 Å cutoff of the mW force field. The interactions between the water molecules and the particles of the pore are described by the potential of eq 1, but adopting different values for ε, λ and A, to modulate the interactions with the water molecules contained in it (see section 2.4). In addition, the molecules of the wall interact with their first neighbors through soft harmonic potentials, as implemented in previous studies.[39,40] This protocol preserves the overall structure of the pore matrix while allowing for vibrations around the corresponding equilibrium positions. The systems considered in this work contained from 2500 particles (empty pores) up to 4000 particles (filled pores). We refer the reader to the Supporting Information for a discussion on the suitability of these model systems to represent silica pores.

Contact Angle. The hydrophobicity of the pore can be tuned in our model through the variation of the parameters ε and λ, which determine the magnitude of the water−wall interaction in the two body term, and the stability of tetrahedral "hydrogen-bonded configurations". To some extent, our procedure is similar in concept to that adopted by Debenedetti and co-workers to obtain different hydrophilicities: by rescaling the charges, they change the ability of the surface to hydrogen bond with water and diminish the overall interaction with water.[57,58] We have characterized the hydrophobicity of the surface in terms of the contact angle, θ, which we have estimated from simulations of droplets on flat surfaces employing the procedure proposed in ref 57. More specifically, NVT molecular dynamics runs of an aggregate of 1192 water molecules were carried out for 10 ns on a planar surface of area 9 × 9 nm^2, with the same amorphous structure as the pore walls.[54] The value of θ was straightforwardly computed from the radial density profile of the water droplet, taking the angle subtended between the profile boundary of the droplet with respect to the solid−liquid interface.

Sorption Isotherms. Adsorption and desorption isotherms were computed in the grand canonical ensemble at 298 K. The usual procedure was followed, in which the adsorption (desorption) branch is built from a series of simulations at various fixed chemical potentials, taking a snapshot from a thermalized run as the starting configuration for the calculation of the next point in the curve, corresponding to a slightly higher (lower) value of μ. Simulations times were between 10 and 25 ns for a single condition (a data-point in the isotherm), in order to obtain a converged density average at the given chemical potential. Pressure and chemical potential were related by assuming the vapor to be an ideal gas.[48] Isotherms are reported in terms of the relative pressure P/P_0, where P_0 is the vapor pressure of the bulk liquid phase of the water model at 298 K. The procedure to compute P_0 is described in detail in refs 55 and 56. Given the absence of rotational degress of freedom in mW, the vapor pressure of the model turns out to be 0.5 mbar, much lower than the experimental value, of 31.6 mbar.[55] The monatomic nature of the mW particles entails a loss of rotational entropy that is more significant in the gas phase than in the liquid, where rotations of atomistic water are impaired. As a consequence, in the coarse-grained water there is a reduction of the free energy gap between the condensed and gas phases, that becomes manifest in a vapor pressure downshift. We have shown elsewhere[55] that this difference

dx.doi.org/10.1021/jp5000396 | J. Phys. C 2014, 118, 16290−16300

Table 1. Contact Angle (θ), Equilibrium Desorption Pressure (P_d), Capillary Condensation Pressure (P_c), Surface Densities, and Adsorption Energies (E_{ads}) as a Function of the mW Parameters ε, λ, and A (see eq 1)[a]

ε (kcal/mol)	λ	θ (deg)	P_d/P_0	P_c/P_0	Γ_{eq}	Γ_c (nm^{-2})	E_{ads} (kcal/mol)
6.19	23.15	0	0.44	0.59	3.4	6.4	13.3
5.56	23.15	9.30	0.53	0.74	1.6	2.5	11.7
6.19	23.15	19.0[b]	0.57	0.75	1.5	2.3	12.6
0.55	0.0	24.4	0.6	1.95	1×10^{-4}	9×10^{-4}	4.1
0.45	0.0	63.4	0.8	4.0	~0[c]	~0[c]	3.1
0.35	0.0	82.9	1.0	6.0	~0[c]	~0[c]	2.3

[a]Γ_{eq} and Γ_c represent, respectively, the surface density in equilibrium and just before condensation. [b]This contact angle was obtained modifying the parameter A to 6.75. [c]Surface density was indistinguishable from zero in the simulations.

between the experimental value P_{exp} and the saturation pressure of the model, P_{mW}, arises from the difference between excess chemical potentials, μ_{xs}:

$$RT \ln\left(\frac{P_{exp}}{P_{mW}}\right) = \mu_{xs}^{exp} - \mu_{xs}^{mW} \quad (2)$$

However, this shift does not affect the accuracy of the mW model to describe the liquid–vapor equilibrium in terms of relative pressure.[55,56] The coexistence curve is in excellent agreement with experiments, whereas the evaporation relative pressures of water aggregates are the same as resulting from the atomistic SPC/E force-field.[55]

RESULTS AND DISCUSSION

Modulation of the Contact Angle through the Water-Surface Potential. We studied pores of 2.8 nm diameter with two different kind of surfaces, respectively, with and without the ability to establish hydrogen bonds with the water molecules. Each of these groups encompasses different ranges of contact angles, from 0 to 19° in the former group, and from 24.4° to 82.9° in the second. As stated above, the parameters ε and λ determine the magnitude of the two- and three-body terms in eq 1. Table 1 shows the contact angle arising from different combinations of ε, λ, and A, while the corresponding droplet profiles are plotted in Figure 1 (the modification of the parameters affect only the interactions between the water molecules and the particles of the pore wall, leaving intact the interaction between water molecules). It can be noticed that outside the very hydrophilic regime, for $\theta > 24°$, λ is set to zero, and there are no hydrogen bonds between water and the pore. Since the parameter λ encourages hydrogen bonds via a repulsive interaction, ε adopts higher values when λ is not zero, to compensate for the destabilizing effect of the three-body term. Additionally, a pore with hydrogen-bonding ability and θ = 19° can be obtained by modifying the value of the A parameter. The adsorption energies (E_{ads}) listed in Table 1 were calculated with two different schemes: (i) from the canonical partition functions obtained via Monte Carlo sampling, and (ii) from the average energy of a molecular dynamics simulation of a single water molecule inside the pore. Both approaches lead to almost identical results. It is intersting to note that, with the present combination of parameters, a substantial decrease in adsorption energy—from nearly 12 to 4 kcal/mol—may be associated with a small change in contact angle—from 19° to 24.4°. Furthermore, it can be seen that there is no monotonic correspondence between contact angle and adsorption energy: the value of E_{ads} is higher for the pore with θ = 19° than for θ = 9.3°. The parameter ε affects both the two and the three-body terms in the potential, meaning that the hydrogen bonds with the surface are partially affected in the pore with θ = 9.3°, whereas they are not in the pore with θ = 19°. Thus, the value of the contact angle does not follow the adsorption energy, but it seemingly arises from the combination of this magnitude and the strength of the interfacial hydrogen bonding.

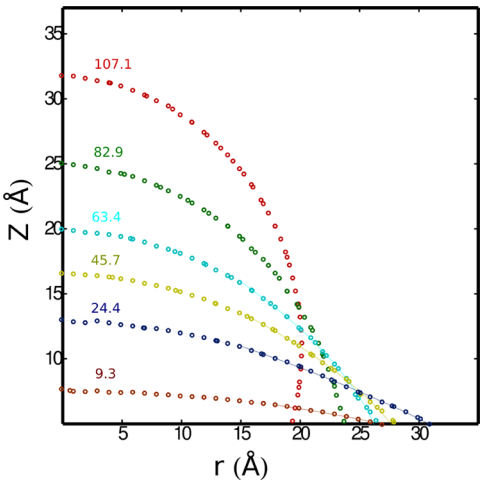

Figure 1. Average profiles for water droplets on a flat surface with different water-wall potentials (tabulated in Table 1). The resulting contact angles are indicated next to each of the curves.

Even if both contact angle and adsorption energy are directly related to the free energy of the fluid–surface interaction, the relation between θ and E_{ads} is by no means direct, nor is it straightforward to establish accurately from fundamental considerations. The adsorption energy as defined in this work is the interaction of water molecules with the cylindrical pore at zero coverage, whereas the contact angle, according to Young's equation, depends on three interfacial tensions: gas–liquid, gas–solid, and solid–liquid. In particular, the latter is neither directly related to the adsorption energy since it is also determined by the interaction of the fluid with itself. Interestingly, however, Werder and co-workers have shown for SPC/E water on a graphite surface that, as far as the fluid does not completely wet the surface, there is a linear relationship between the contact angle and the adsorption energy, and also between the adsorption energy and the parameter ε corresponding to the C–O interaction in the Lennard–Jones potential, therefrom a direct relation between ε and the contact angle also holds.[59]

As a matter of fact, the same kind of linear relationship can be recognized in our data, when only one of the parameters in the potential is varied at a time. For example, an inspection of the last three rows of Table 1 reveals that for fixed values of λ

dx.doi.org/10.1021/jp5000396 | J. Phys. Chem. C 2014, 118, 16290–16300

and A, the adsorption energy increases approximately linearly with ε, whereas the contact angle shows a linear decrease. To explore this further, we have analyzed the dependence of contact angle and adsorption energy on one of the relevant parameters used to tune the interaction, λ, ε, or A, while keeping constant the other two. The results, summarized in Figure S1 included in the Supporting Information, reveal an almost linear relation of θ with respect to E_{ads} within a wide range of conditions. For the case of $\lambda = 0$, our data resemble the results from atomistic simulations.[59] Beyond this agreement, the interesting point is that different combinations of hydrogen bonding and strengths of the two-body term may lead to the same contact angle and even to the same adsorption energy. In other words, different materials may exhibit comparable contact angles, in spite of having a different adsorption energy. However, it is seemingly the latter variable that is the most relevant one in determining the condensation pressure.

Equilibrium Desorption Pressure and the Kelvin Equation. In open-ended, uniform cylindrical pores, desorption consists of the evaporation of the confined fluid at the liquid−gas interface and is assumed to take place in equilibrium.[9,30] To obtain the liquid−vapor equilibrium pressure, we constructed the desorption branch of the isotherm performing simulations that start with partially filled pores, which expose a liquid−vapor interface where evaporation may proceed as in open-ended pores. The isotherms for a varierty of contact angles are displayed in Figures 2 and 3. We found that

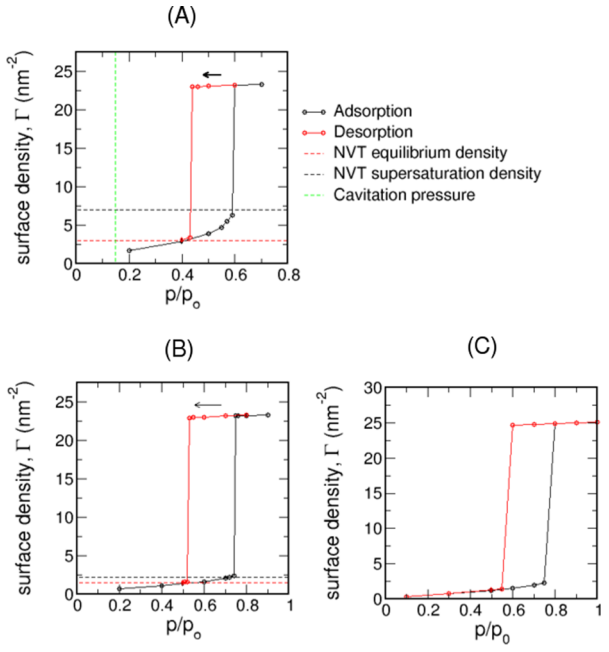

Figure 2. Water sorption isotherms obtained in pores with contact angles 0° (A), 9.3° (B), and 19° (C). The horizontal dashed lines indicate the results from canonical molecular dynamics simulations for the density of the surface adsorbed phase in equilibrium (red) and at the point of condensation (black).

the surface density of water molecules at the liquid−vapor equilibrium point, Γ_{eq}, is strongly dependent on the hydrophilicity of the pore. It changes from 3.4 nm^{-2} for $\theta = 0$, to nearly zero for $\theta = 82.9°$ (Table 1). The surface densities calculated in canonical simulations are indicated in Figure 2 with red horizontal dashed lines. A higher hydrophilicity of the interface favors the stabilization of thicker adsorbed layers

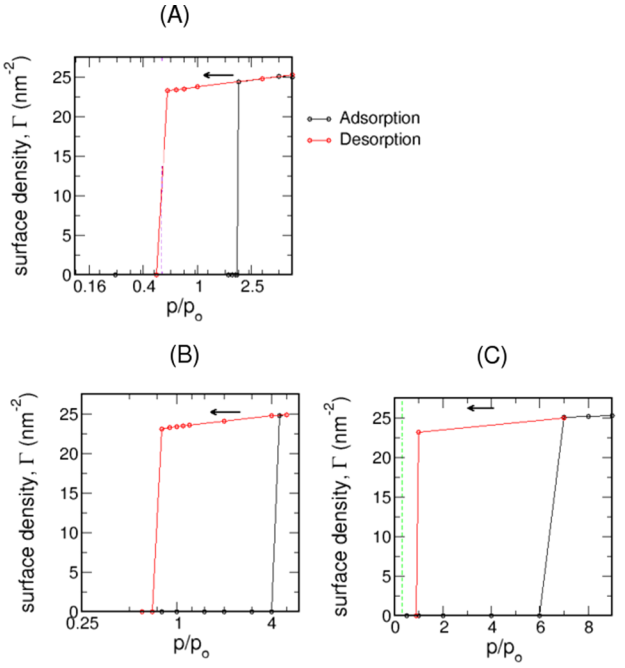

Figure 3. Water sorption isotherms obtained in pores with contact angles 24.4° (A), 63.4° (B), and 82.9° (C). The vertical green dashed line in panel (C) indicates the cavitation pressure.

against the formation of a condensed phase at a given pressure. The equilibrium surface densities obtained through GCMD simulations are in good agreement with the surface densities of water reported in our previous molecular dynamics simulations in the canonical ensamble,[39,40] which will be discussed below in the context of the present results.

Remarkably, the equilibrium desorption pressures P_d obtained for the pores of different hydrophilicities (Table 1) are accurately predicted by the Kelvin equation:

$$\ln \frac{P_d}{P_0} = -\frac{2\sigma V_m \cos(\theta)}{RTr} \quad (3)$$

where σ and V_m are the liquid−vapor surface tension and the molar volume of the liquid, r is the pore radius, R is the universal gas constant, and T is the temperature. In Figure 4 the logarithm of the desorption pressure resulting from our GCMD

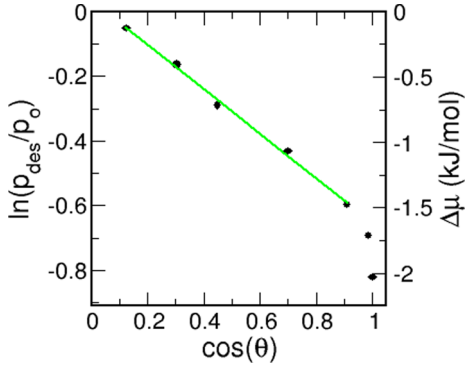

Figure 4. Logarithm of the relative desorption pressure as a function of the cosine of the contact angle θ. The linear dependence indicates that the Kelvin equation is satisfied for contact angles above 20°. The green line guides the eye; from its slope, the surface tension of the mW model is recovered.

dx.doi.org/10.1021/jp5000396 | J. Phys. Chem. C 2014, 118, 16290−16300

simulations is represented as a function of the cosine of the contact angle. It is seen that these two variables follow a linear relationship for values of θ above 20°. Moreover, by inserting the molar volume of liquid water, the surface tension at 298 K can be calculated from the slope of the curve. The outcome is 0.066 N/m, in perfect agreement with the surface tension reported for the mW model,[38] which is in turn close to the experimental value of 0.071 N/m.[60] The right axis in Figure 4 shows the variation in terms of $\Delta\mu_d = RT \ln(P_d/P_0)$, reflecting how much the free energy of the confined liquid at the evaporation point departs from the corresponding bulk value. The verification of the Kelvin equation confirms that the desorption is taking place in equilibrium, and in fact the same linear relation is not satisfied for the condensation pressures obtained from the adsorption branches, which involve an activated process. It may be quite surprising to find that the validity of the Kelvin equation extends to water in pores of 2.8 nm diameter. In recent work, we have found that the vapor pressure of water nanodroplets obeys the Kelvin equation down to diameters of 2 nm.[56] It must be recalled that density functional theory calculations and lattice models dating back to more than 20 years ago have indicated that the Kelvin equation describes the equilibrium transition pressures of Lennard–Jones fluids in pores of only six molecular diameters.[61,62] The reason why this macroscopic theory holds down to this nanoscopic scale is not yet clear. Evans noted that the Kelvin equation is valid as long as the fluid–wall interaction is weak enough to prevent wetting,[63] which is consistent with the deviations observed in Figure 4 for low contact angles. When the liquid wets the walls completely, strong deviations from the Kelvin relation may be expected theoretically[64,65] and have in fact been found in lattice and continuum models simulations—of up to 40% in terms of relative pressure.[66,67] These deviations are typically adscribed to the development of thick layers that reduce the effective diameter of the pore or to interactions that affect the shape of the meniscus.[63] However, we do not observe very thick adsorbed layers in our simulations: even for the most hydrophilic pore the equilibrium surface coverage is not above a monolayer.

Nonequilibrium Filling and the Effect of Hydrophobicity. Figure 2 depicts the isotherms calculated in pores of 2.8 nm diameter with the capability to form hydrogen bonds with water (λ = 23.15), for θ = 0°, θ = 9.3°, and θ = 19°. All of them present hysteresis loops of type H1, as expected for homogeneous cylindrical pores of this size.[9] For a contact angle equal to zero, capillary condensation is observed at P/P_0 = 0.59, concurring with a water surface density Γ_c = 6.4 nm^{-2}. Desorption, on the other hand, takes place at $P/P_0 \approx 0.44$, with a surface coverage Γ_{eq} = 3.4 nm^{-2}. This isotherm shows good agreement with experimental measurements performed in hydroxylated silica mesopores of comparable diameter like MCM-41, FSM-16, or MCM-48.[10,68−70] The contact angle in the inner surface of these materials is usually unknown, but it is assumed to be close to zero for a high degree of hydroxylation, when the silanol surface density is around 3 nm^{-2} or above.[71] For these silica pores the adsorption branch is generally found somewhere in the P/P_0 range between 0.5 and 0.7,[10,70] with desorption typically shifted 0.1 to lower pressures. The adsorption–desorption hysteresis resulting from our simulations is slightly larger than usually seen in experiments. We attribute this to two major reasons: (i) most mesoporous materials exhibit a distribution of pore sizes—rather than a uniform pore diameter—that becomes manifest in the slope of the adsorption branch, which, far from being vertical, may sweep up to two tenths in units of relative pressure; and (ii) capillary condensation in these pores is an out of equilibrium, activated phenomenon, which may require higher chemical potentials in simulations than in experiments, in view of the different accessible sampling times. We note that the water surface density at the point of condensation, 6.8 nm^{-2} in our calculations, is identical to the 6.8 nm^{-2} value estimated for hydroxylated FSM-16 silica.[10]

The increase in the contact angle causes the shift of the adsorption and desorption branches toward higher pressures. In turn, there is also a rise in the water surface density at the condensation point with respect to the equilibrium density. As we have discussed in previous studies in the canonical ensemble,[39,40] a large supersaturation of the surface is needed in hydrophilic pores of this diameter to unleash capillary condensation. The present simulations indicate that for θ = 0 the surface adsorbed phase must reach nearly twice its equilibrium value to produce condensation.

Remarkably, these results are in excellent agreement with the surface densities of water found in our previous molecular dynamics simulations at a constant number of particles (NVT).[39,40] Canonical molecular dynamics show that for $N_c < N < N_{100\%}$ (where N_c and $N_{100\%}$ refer, respectively, to the number of molecules at the point of condensation and at conditions of full filling), the water molecules inside the pore separate into two phases: a low density, surface adsorbed phase, and a liquid-like phase. These coexisting states—corresponding to points within the vertical jump in the adsorption isotherm—are difficult to stabilize in grand canonical simulations, which lead to a single phase, adsorbed or liquid-like, depending on whether the ratio P/P_0 is below or above the capillary condensation relative pressure. However, the water surface density obtained in the NVT ensemble for a filling just below N_c matches the one at the point of condensation seen in the μVT simulations ($\approx$ 7 nm^{-2}). In the same way, the water density of the surface adsorbed phase in equilibrium with the condensed phase observed for $N_c < N < N_{100\%}$ in the canonical simulations ($\approx$ 3 nm^{-2}) agrees well with that found for the desorption branch in the grand canonical framework. This clearly shows that for this system the NVT simulations are able to capture the same equilibrium and metastable states described by the μVT isotherm. An in-depth discussion concerning the incidence of the ensemble and reservoir size on sorption isotherms has been elaborated by Puibasset, Kierlik and Tarjus.[72,73]

Figure 3 presents the isotherms obtained for pores where the possibility of establishing hydrogen bonds with the surface has been obliterated by setting λ = 0 (see Table 1). For a 2.8 nm pore with a contact angle of 24°, adsorption only occurs for a pressure significantly above the saturation pressure of the bulk fluid. This is because the surface density does not reach a value that can lead to nucleation of a liquid phase even at high supersaturation. Table 1 shows that on the pores where the water–surface interaction is weaker than the interaction of water with itself (contact angles of 24.4° and above), the equilibrium and condensation densities Γ_{eq} and Γ_c exhibit a dramatic decrease with respect to the more hydrophilic pores. Moreover, Figure 2 and Table 1 indicate that an increase in θ affects the condensation pressure (P_c) to a higher extent than the desorption pressure (P_d). In other words, hydrophobicity enlarges the hysteresis loop. Figure 5 displays the difference between the chemical potentials at the condensation and the

dx.doi.org/10.1021/jp5000396 | J. Phys. Chem. C 2014, 118, 16290−16300

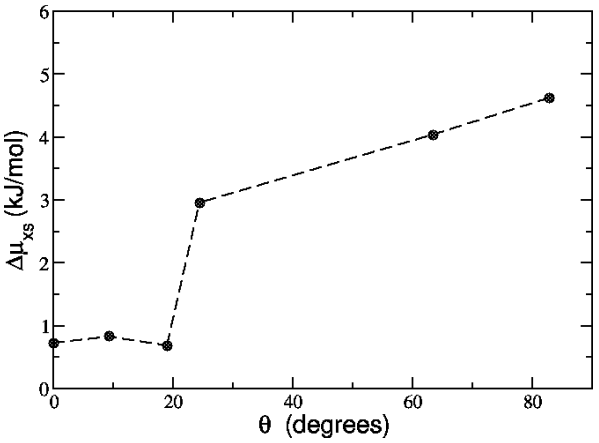

Figure 5. Excess chemical potential at the point of condensation ($\Delta\mu_{xs}$) as a function of the contact angle θ. The value of $\Delta\mu_{xs}$ reflects the lowering in the stabilization provided by the surface to the formation of the critical droplet (see text).

desorption points, $\Delta\mu_{xs} = \mu_c - \mu_d = RT \ln(P_c/P_d)$, as a function of the contact angle. The value of $\Delta\mu_{xs}$ represents the excess chemical potential of liquid with respect to gas at the point of condensation, which is equal to the nucleation free energy barrier plus the surface contributions. $\Delta\mu_{xs}$ rises from about 0.2 kcal/mol (1/3 of kT) for $\theta < 20°$, to 0.7 kcal/mol ($1.1kT$) for $\theta = 24.4°$, and continues to increase slowly with the contact angle. This behavior is consistent with a heterogeneous condensation mechanism where the interactions with the surface largely determine the nucleation barrier. Instead, the nature of the wall has seemingly a smaller influence on the equilibrium desorption process, consisting of the evaporation from the homogeneous liquid–vapor interface. In particular, these results show that the contact angle alone does not determine the capillary condensation point and hysteresis. Figure 5 reveals an abrupt change in $\Delta\mu_{xs}$ associated with a drop of more than 7 kcal/mol in the adsorption energy, though the contact angle hardly increases. Hence, in uniform pores of this size, the water surface affinity plays an essential role in the nucleation step, becoming a more important descriptor than the contact angle. The development of an adsorbed layer appears to be essential to nucleate the condensed phase. This results from the mechanism of condensation requiring a significant density of water at the surface, that is not achieved below a minimum value of E_{ads}.

Figure 3C illustrates the water isotherm for a 2.8 nm pore with $\theta = 82.9°$. This contact angle roughly represents the interaction of water with a graphitic material. According to our simulations, condensation of water should occur in these systems in conditions of vapor supersaturation. This observation is fully consistent with the experimental evidence presented by Easton and Machin[20] and discussed at length by Monson.[45,47] A large body of experimental data exists on water adsorption on porous carbons, exhibiting a varied range of behaviors owing to differences in the density of active surface groups, pore size distribution, and topology, all variables that are often poorly characterized (see, for example, the review by Brennan and co-workers[19]). In particular, experiments in graphitized carbon black, where the contact angle is approximately 85°, have shown adsorption and desorption pressures, respectively, slightly above and below the bulk liquid–vapor transition pressure.[20] Independent molecular simulation studies by different groups, including those of Brennan,[43] Monson,[45,47] Wang,[74] and Bhatia,[75] support this result: in highly hydrophobic pores, nucleation of water is a homogeneous process, occurring at a pressure close to or above P_0. Condensation below P_0 is only possible in the presence of active surface sites[21,42−44] that support the buildup of water density at the surface of the pore. A strict quantitative comparison between the experimental and simulated isotherms, however, is not straightforward for these kind of systems, since the graphitic samples do not contain independent cylindrical pores of homogeneous diameter, and heterogeneity and pore connectivity will eventually determine the exact value of the capillary condensation pressure. It is also important to emphasize that the presence of liquid outside the pore—for example, in a connected reservoir or cavity—would inevitably nucleate the liquid when P exceeds P_0, and result in the adsorption of water in the pore, shifting P_c to lower pressures. To show this, we conducted simulations in finite hydrophobic pores, including a liquid phase in the exterior, as illustrated in Figure 6. When the pressure reaches P_0, water condenses on the

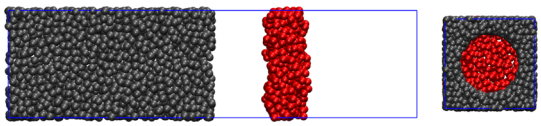

Figure 6. Model of the pore with a water reservoir in the outer part (side and front views). Gray: particles of the pore. Red: molecules of the liquid phase. The blue line marks the boundaries of the simulation box.

bulk liquid, which grows and reaches the boundary of the pore. In these conditions, the filling of the pore occurs with no activation barrier, at pressures slightly above P_0, i.e., much lower than in the absence of the liquid.

Our GCMD approach delivers a dynamical description of the condensation process in real time. The inspection of the structures next to the transition point reveal fundamentally different mechanisms for the nucleation of the liquid phase, depending on the water–surface interaction. In the hydrophilic case, the filling of the pore is heterogeneous. Above certain surface density (of around 7 nm^{-2} for this pore diameter), a fluctuation closes the gap across the center of the pore and the liquid is formed. As the contact angle is increased, this mechanism leaves room to a different path, involving the formation of a droplet that grows in a certain spot on the surface. Clearly, water molecules are more stable as part of an aggregate than adsorbed on the moderately hydrophobic pore-wall. Finally, in a highly hydrophobic environment representing a graphitized carbon free of active sites, the nucleation process does not significantly differ from the homogeneous nucleation of liquid from the vapor phase. The weak interactions with the surface have very little impact on the development of the nuclei necessary for condensation, and the transition takes place close to the vapor spinodal. Figure 7 displays a temporal sequence of images extracted from the GCMD simulations illustrating these mechanisms of condensation for $\theta = 0°$ and $\theta = 9.3°$. These configurations resemble the morphologies reported by Men et al.[74] for the critical nuclei leading to adsorption in square pores of various fluid–wall interactions, on the basis of lattice density functional theory. It is worth noticing that these observed mechanisms are in line with our previous findings from canonical molecular dynamics simulations.[40] In fact, the two

dx.doi.org/10.1021/jp5000396 | J. Phys. Chem. C 2014, 118, 16290−16300

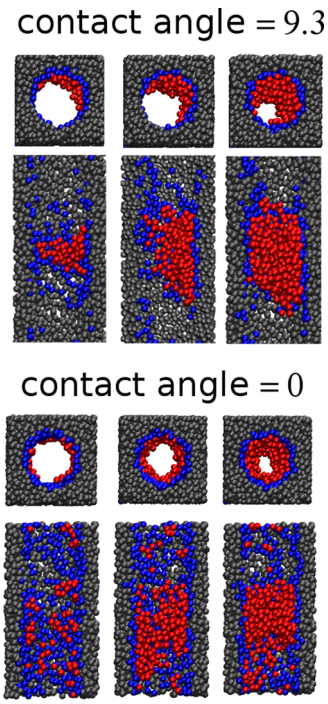

Figure 7. Front and side cross-section views of the pore model depicting two different nucleation mechanisms. From left to right, temporal sequence of snapshots taken from the molecular dynamics simulations at the condensation pressure. Gray: particles of the pore. Blue: water molecules adsorbed on the surface. Red: the rest of the water molecules.

frameworks (NVT and μVT) are complementary: the canonical simulations offer insights on the points along the adsorption jump that are not easily stabilized in the grand canonical ensamble; on the other hand, the present simulations establish the pressure corresponding to the different fillings obtained in the molecular dynamics calculations.

Nonequilibrium Desorption: Cavitation. In the absence of a liquid−vapor interface, as in the case of blocked-ends pores, desorption becomes an activated process involving the nucleation of a bubble inside the condensed phase.[9] This phenomenon, known as cavitation, leads to very low desorption pressures. We studied the cavitation effect by gradually decreasing the chemical potential in completely filled pores. This type of desorption, indicated with green vertical dashed lines in Figures 2A and 3C, occurs at $P/P_0 \approx 0.2$.

Interestingly, the cavitation follows different mechanisms in the systems represented in Figures 2A and 3C, corresponding to contact angles of 0° and 82.9° respectively. In the hydrophilic pore, the nucleation of the bubble is a homogeneous process mainly controlled by the intermolecular forces in the condensed phase. In the hydrophobic pore, instead, the cavity tends to form in contact with the wall. Figure 8 depicts the evolution of the desorption dynamics around the cavitation pressure in the absence of a liquid−vapor interface. The images show cross section views of the pore along the main axis, in a temporal sequence. Water molecules at different distances from the pore center are displayed in different colors. It can be seen that in the hydrophobic pore the bubble nucleates heterogeneously at the surface, whereas it forms homogeneously in the hydrophilic system. Curiously, this drastic change in mechanism determines only a minor shift in the cavitation relative pressures, from 0.15 in the hydrophilic to

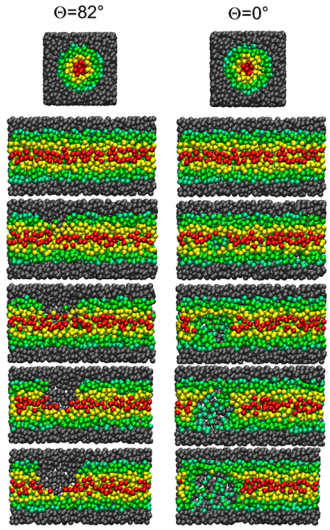

Figure 8. Front and side cross-section views of the pore model depicting two different cavitation mechanisms: heterogeneous (left) and homegeneous (rigth). From top to bottom, temporal sequence of snapshots taken from the molecular dynamics simulations at the cavitation pressure. For clarity, water molecules are displayed in different colors according to their distance to the wall. The particles of the pore wall are represented in gray.

0.25 in the hydrophobic cases, which represents a chemical potential difference of only 0.3 kcal/mol. The dependence of this property on the water−surface affinity is therefore much weaker than in the case of P_c. This may be explained by noting that adsorption depends on the buildup of water at the surface, which is related to the hydrophilicity, although not specifically the contact angle. Desorption, on the other hand, requires the nucleation of a vacuum bubble from the liquid, and the formation of a dewetted, vapor-like surface, can only occur on truly hydrophobic interfaces (i.e., contact angle $\gg$ 90°).

CONCLUSIONS

We have studied sorption of water in cylindrical pores of 2.8 nm, to elucidate how the condensation and desorption pressures P_c and P_d depend on the contact angle θ and the adsorption energy E_{ads}. In the first place, we showed that desorption in open-ended pores is a nonactivated process in which pressure is accurately described by the Kelvin equation, with deviations occurring for contact angles below 20°. This result is in agreement with early simulations of Lennard−Jones fluids in nanopores, indicating that the Kelvin equation is verified in pores of a few molecular diameters, providing there is no full wetting.[61−63] It would be very interesting to explore the range of applicability and to understand the microscopic reasons behind the success of eq 3 to describe the behavior in the nanoscale. To some extent, these questions have been the subject of recent research by our group,[56] and the conclusions obtained in that work can possibly provide an explanation in the present systems.

On the other hand, our simulations indicate that for the most hydrophilic pores the decrease in contact angle affects both P_c and P_d to similar extents, while on the more hydrophobic surfaces a decrease in θ has a much larger impact on the condensation than on the desorption vapor pressure. The reason for this can be found in the nucleation mechanism of the liquid phase, which requires a significant density of water at the surface that cannot be achieved on the pores with little affinity

dx.doi.org/10.1021/jp5000396 | J. Phys. Chem. C 2014, 118, 16290−16300

for H_2O. This is reflected in the correlation between the adsorption pressure P_c and the density at the point of condensation Γ_c (Table 1), whereas a similar correlation does not exist between P_d and Γ_{eq}. When the interaction of water with the surface becomes weaker than the interaction with itself, decreasing from approximately 12 to 4 kcal/mol, a change in 3 orders of magnitude is observed in the surface density, accompanied by a 4-fold increase in the excess chemical potential. This is associated with a variation of only 5° in θ. Hence, we conclude that the contact angle is not the determining factor of the adsorption pressure. The effect of hydrophobicity is to separate the adsorption from the desorption branch, enlarging the hysteresis.

In experimental isotherms of carbonaceous solids, capillary condensation is rarely seen at pressures much higher than P_0. In contrast, we have found that in hydrophobic pores P_c can be several times larger than P_0. We conjecture that the reason for this apparent disagreement is the difficulty to prevent condensation in an experimental setup when P exceeds the saturation value. Once the first droplet of liquid is formed in the adsorption chamber, it percolates through the material, and the pores can be filled at P_0 with no activation barrier.

Finally, it is worth noticing that simulations in the NVT and μVT ensemble predict identical values of the surface densities in equilibrium and at condensation. As we argued in previous work,[41] this confirms that canonical molecular dynamics can describe the transition and the equilibrium states with the same accuracy as grand canonical simulations. Moreover, modeling in the canonical ensemble can stabilize the liquid−vapor coexisting states along the adsorption ramp. These states are difficult to obtain in a grand canonical setting, where only one phase may be observed at a time. The canonical approach, however, does not provide a link to the pressure or chemical potential, and thus both frameworks become complementary.

■ ASSOCIATED CONTENT

Supporting Information

Details on the definition of pore diameter, a discussion of the suitability of the present models to represent experimental silica pores, and the dependence of the contact angle on the adsorption pressure as a function of a single interaction parameter. This material is available free of charge via the Internet at http://pubs.acs.org.

■ AUTHOR INFORMATION

Corresponding Author

*E-mail: damian@qi.fcen.uba.ar.

Notes

The authors declare no competing financial interest.

■ ACKNOWLEDGMENTS

We are grateful to Prof. Peter Monson for valuable discussions. This study has been supported by a collaborative grant of the Agencia Nacional de Promocion Cientifica y Tecnologica de Argentina, PICT 2012-2292 to V.M. and D.A.S., and by funding from the University of Buenos Aires, UBACyT 20020120100333BA. We acknowledge the Center of High Performance Computing of the University of Utah for technical support and the allocation of computing time.

■ REFERENCES

(1) Cohen, L. H. Hysteresis and the Capillary Theory of Adsorption of Vapors. *J. Am. Chem. Soc.* **1944**, *66*, 98−105.
(2) Emmett, P. H. Adsorption and Pore-Size Measurements on Charcoals and Whetlerites. *Chem. Rev.* **1948**, *43*, 69−148.
(3) Katz, S. M. Permanent Hysteresis in Physical Adsorption. *J. Phys. Colloid Chem.* **1949**, *53*, 1166−1186.
(4) Everett, D. H.; Whitton, W. I. A General Approach to Hysteresis. *T. Faraday Soc.* **1952**, *48*, 749.
(5) Everett, D. H.; Haynes, J. M. Model Studies of Capillary Condensation. 1. Cylindrical Pore Model with Zero Contact Angle. *J. Colloid Interface Sci.* **1972**, *38*, 125−137.
(6) Derjaguin, B. V. *Prog. Surf. Sci.* See a selected compilation in Vol. *45*.
(7) Defay, R.; Prigogine, I. *Surface Tension and Adsorption*, 1st ed.; Longmans: London, 1966.
(8) Rouquerol, F.; Rouquerol, J.; Sing, K. *Adsorption by Powders and Porous Solids*, 1st ed.; Academic Press: New York, 1999.
(9) Thommes, M. Physical Adsorption Characterization of Nanoporous Materials. *Chem. Ing. Technol.* **2010**, *82*, 1059−1073.
(10) Inagaki, S.; Fukushima, Y. Adsorption of Water Vapor and Hydrophobicity of Ordered Mesoporous Silica, FSM-16. *Microporous Mesoporous Mater.* **1998**, *21*, 667−672.
(11) Gregg, S. J.; Sing, K. S. W. *Adsorption, Surface Area and Porosity*, 2nd ed.; Academic Press: New York, 1982.
(12) Branton, P. J.; Hall, P. G.; Treguer, M.; Sing, K. S. W. Adsorption of Carbon Dioxide, Sulfur Dioxide and Water Vapour by MCM-41, a Model Mesoporous Adsorbent. *J. Chem. Soc., Faraday Trans.* **1995**, *91*, 2041−2043.
(13) Llewellyn, P. L.; Schueth, F.; Grillet, Y.; Rouquerol, F.; Rouquerol, J.; Unger, K. K. Water Sorption on Mesoporous Aluminosilicate MCM-41. *Langmuir* **1995**, *11*, 574−577.
(14) Llewellyn, P.; Grillet, Y.; Schuth, F.; Reichert, H. Effect of Pore Size on Adsorbate Condensation and Hysteresis Within a Potential Model Adsorbent: M41S. *Microporous Mater.* **1994**, *3*, 345−349.
(15) Ravikovitch, P. I.; O Domhnaill, S. C.; Neimark, A. V.; Schuth, F. S.; Unger, K. K. Capillary Hysteresis in Nanopores: Theoretical and Experimental Studies of Nitrogen Adsorption on MCM-41. *Langmuir* **1995**, *11*, 4765−4772.
(16) Matsumoto, A.; Sasaki, T.; Nishimiya, N.; Tsutsumi, K. Evaluation of the Hydrophobic Properties of Mesoporous FSM-16 by Means of Adsorption Calorimetry. *Langmuir* **2001**, *17*, 47−51.
(17) Takahara, S.; Nakano, M.; Kittaka, S.; Kuroda, Y.; Mori, T.; Hamano, H.; Yamaguchi, T. J. Neutron Scattering Study on Dynamics of Water Molecules in MCM-41. *J. Phys. Chem. B* **1999**, *103*, 5814−5819.
(18) Grunberg, B.; Emmler, T.; Gedat, E.; Shenderovich, I.; Findenegg, G.; Limbach, H.-H.; Buntkowsky, G. Hydrogen Bonding of Water Confined in Mesoporous Silica MCM-41 and SBA-15 Studied by 1H Solid-State NMR. *Chem.—Eur. J.* **2004**, *10*, 5689−5696.
(19) Brennan, J. K.; Bandosz, T. J.; Thomson, K. T.; Gubbins, K. E. Water in Porous Carbons. *Colloids Surf. A—Physicochem. Eng. Aspects* **2001**, *187*, 539−568.
(20) Easton, E. B.; Machin, W. D. Adsorption of Water Vapor on a Graphitized Carbon Black. *J. Colloid Interface Sci.* **2000**, *231*, 204−206.
(21) Tao, Y.; Muramatsu, H.; Endo, M.; Kaneko, K. Evidence of Water Adsorption in Hydrophobic Nanospaces of Highly Pure Double-Walled Carbon Nanotubes. *J. Am. Chem. Soc.* **2010**, *132*, 1214−1215.
(22) Heffelfinger, G. S.; van Swol, F.; Gubbins, K. E. Adsorption Hysteresis in Narrow Pores. *J. Chem. Phys.* **1988**, *89*, 5202−5205.
(23) Ball, P. C.; Evans, R. Temperature Dependence of Gas Adsorption on a Mesoporous Solid: Capillary Criticality and Hysteresis. *Langmuir* **1989**, *5*, 714−723.
(24) Peterson, B. K.; Heffelfinger, G. S.; Gubbins, K. E.; van Swol, F. Layering Transitions in Cylindrical Pores. *J. Chem. Phys.* **1990**, *93*, 679−685.

(25) Papadopoulou, A.; van Swol, F.; Marini Bettolo Marconi, U. Pore-End Effects on Adsorption Hysteresis in Cylindrical and Slitlike Pores. *J. Chem. Phys.* **1992**, *97*, 6942−6952.
(26) Votyakov, E. V.; Tovbin, Y. K.; MacElroy, J. M. D.; Roche, A. A Theoretical Study of the Phase Diagrams of Simple Fluids Confined within Narrow Pores. *Langmuir* **1999**, *15*, 5713−5721.
(27) Monson, P. Understanding Adsorption/Desorption Hysteresis for Fluids in Mesoporous Materials Using Simple Molecular Models and Classical Density Functional Theory. *Micropor. Mesopor. Mater.* **2012**, *160*, 47−66.
(28) Gubbins, K. E.; Liu, Y.-C.; Moore, J. D.; Palmer, J. C. The Role of Molecular Modeling in Confined Systems: Impact and Prospects. *Phys. Chem. Chem. Phys.* **2011**, *13*, 58−85.
(29) Coasne, B.; Hung, F. R.; Pellenq, R. J.-M.; Siperstein, F. R.; Gubbins, K. E. Adsorption of Simple Gases in MCM-41 Materials: The Role of Surface Roughness. *Langmuir* **2006**, *22*, 194−202.
(30) Fan, C.; Do, D. D.; Nicholson, D. On the Cavitation and Pore Blocking in Slit-Shaped Ink-Bottle Pores. *Langmuir* **2011**, *27*, 3511−3526.
(31) Smit, B.; Siepmann, J. I. Simulating the Adsorption of Alkanes in Zeolites. *Science* **1994**, *264*, 1118−1120.
(32) Sant, M.; Leyssale, J.-M.; Papadopoulos, G. K.; Theodorou, D. N. Molecular Dynamics of Carbon Dioxide, Methane and Their Mixtures in a Zeolite Possessing Two Independent Pore Networks as Revealed by Computer Simulations. *J. Phys. Chem. B* **2009**, *113*, 13761−13767.
(33) Smit, B.; Maesen, T. L. M. Molecular Simulations of Zeolites: Adsorption, Diffusion, and Shape Selectivity. *Chem. Rev.* **2008**, *108*, 4125−4184.
(34) Brovchenko, I.; Geiger, A.; Oleinikova, A. Water in Nanopores. I. Coexistence Curves from Gibbs Ensemble Monte Carlo Simulations. *J. Chem. Phys.* **2004**, *120*, 1958−1972.
(35) Shirono, K.; Daiguji, H. Molecular Simulation of the Phase Behavior of Water Confined in Silica Nanopores. *J. Phys. Chem. C* **2007**, *111*, 7938−7946.
(36) Siboulet, B.; Coasne, B.; Dufrêche, J.-F.; Turq, P. Hydrophobic Transition in Porous Amorphous Silica. *J. Phys. Chem. B* **2011**, *115*, 7881−7886.
(37) Schreiber, A.; Bock, H.; Schoen, M.; Findenegg, G. H. Effect of Surface Modification on the Pore Condensation of Fluids: Experimental Results and Density Functional Theory. *Mol. Phys.* **2002**, *100*, 2097−2107.
(38) Molinero, V.; Moore, E. B. Water Modeled As an Intermediate Element between Carbon and Silicon. *J. Phys. Chem. B* **2009**, *113*, 4008−4016.
(39) de la Llave, E.; Molinero, V.; Scherlis, D. A. Water Filling of Hydrophilic Nanopores. *J. Chem. Phys.* **2010**, *133*, 34513.
(40) de la Llave, E.; Molinero, V.; Scherlis, D. A. Role of Confinement and Surface Affinity on Filling Mechanisms and Sorption Hysteresis of Water in Nanopores. *J. Phys. Chem. C* **2011**, *116*, 1833−1840.
(41) Solveyra, E. G.; de la Llave, E.; Soler-Illia, G. J. A. A.; Molinero, V.; Scherlis, D. A. Structure, Dynamics, and Phase Behavior of Water in TiO2 Nanopores. *J. Phys. Chem. C* **2013**, *117*, 3330−3342.
(42) Muller, E. A.; Rull, L. F.; Vega, L. F.; Gubbins, K. E. Adsorption of Water on Activated Carbons: A Molecular Simulation Study. *J. Phys. Chem.* **1996**, *100*, 1189−1196.
(43) Brennan, J. K.; Thomson, K. T.; Gubbins, K. E. Adsorption of Water in Activated Carbons: Effects of Pore Blocking and Connectivity. *Langmuir* **2002**, *18*, 5438−5447.
(44) Striolo, A.; Chialvo, A. A.; Cummings, P. T.; Gubbins, K. E. Simulated Water Adsorption in Chemically Heterogeneous Carbon Nanotubes. *J. Chem. Phys.* **2006**, *124*, 74710.
(45) Liu, J.-C.; Monson, P. A. Does Water Condense in Carbon Pores? *Langmuir* **2005**, *21*, 10219−10225.
(46) Liu, J.-C.; Monson, P. A. Monte Carlo Simulation Study of Water Adsorption in Activated Carbon. *Ind. Eng. Chem. Res.* **2006**, *45*, 5649−5656.
(47) Monson, P. A. Contact Angles, Pore Condensation, and Hysteresis: Insights from a Simple Molecular Model. *Langmuir* **2008**, *24*, 12295−12302.
(48) Frenkel, D.; Smit, B. *Understanding Molecular Simulation*, 2nd ed.; Academic Press: New York, 2002.
(49) Heffelfinger, G. S.; van Swol, F. Diffusion in Lennard-Jones Fluids Using Dual Control Volume Grand Canonical Molecular Dynamics Simulation (DCV-GCMD). *J. Chem. Phys.* **1994**, *100*, 7548−7552.
(50) Arya, G.; Chang, H.-S.; Maginn, E. J. A Critical Comparison of Equilibrium, Non-equilibrium and Boundary-Driven Molecular Dynamics Techniques for Studying Transport in Microporous Materials. *J. Chem. Phys.* **2001**, *115*, 8112−8124.
(51) Cracknell, R. F.; Nicholson, D.; Quirke, N. Direct Molecular Dynamics Simulation of Flow Down a Chemical Potential Gradient in a Slit-Shaped Micropore. *Phys. Rev. Lett.* **1995**, *74*, 2463−2466.
(52) Plimpton, S. Fast Parallel Algorithms for Short-Range Molecular Dynamics. *J. Comput. Phys.* **1995**, *117*, 1−19.
(53) Moore, E. B.; Molinero, V. Structural Transformation in Supercooled Water Controls the Crystallization Rate of Ice. *Nature* **2011**, *479*, 506−508.
(54) Moore, E. B.; Allen, J. T.; Molinero, V. Liquid-Ice Coexistence below the Melting Temperature for Water Confined in Hydrophilic and Hydrophobic Nanopores. *J. Phys. Chem. C* **2012**, *116*, 7507−7514.
(55) Factorovich, M.; Molinero, V.; Scherlis, D. A. A Simple Grand Canonical Approach to Compute the Vapor Pressure of Bulk and Finite Size Systems. *J. Chem. Phys.* **2014**, 064111.
(56) Factorovich, M.; Molinero, V.; Scherlis, D. A. Vapor Pressure of Water Nanodroplets. *J. Am. Chem. Soc.* **2014**, 4508−4514.
(57) Giovambattista, N.; Debenedetti, P. G.; Rosky, P. J. Effect of Surface Polarity on Water Contact Angle and Interfacial Hydration Structure. *J. Phys. Chem. B* **2007**, *111*, 9581−9587.
(58) Giovambattista, N.; G, P.; Rosky, P. J.; Debenedetti, P. G. Effect of Temperature on the Structure and Phase Behavior of Water Confined by Hydrophobic, Hydrophilic, and Heterogeneous Surfaces. *J. Phys. Chem. B* **2009**, *113*, 13723−13734.
(59) Werder, T.; Walther, J. H.; Jaffe, R. L.; Halicioglu, T.; Koumoutsakos, P. On the Water-Carbon Interaction for Use in Molecular Dynamics Simulations of Graphite and Carbon Nanotubes. *J. Phys. Chem. B* **2003**, *107*, 1345−1352.
(60) *CRC Handbook of Chemistry and Physics*, 81st ed.; CRC Press: Boca Raton, FL, 2000−2001.
(61) Tarazona, P.; Marini Bettolo Marconi, U.; Evans, R. Phase Equilibria of Fluid Interfaces and Confined Fluids. *Mol. Phys.* **1987**, *60*, 573−595.
(62) Bruno, E.; Marini Bettolo Marconi, U.; Evans, R. Phase Transitions in a Confined Lattice Gas: Prewetting and Capillary Condensation. *Physica A* **1987**, *141*, 187−210.
(63) Evans, R. Fluids Adsorbed in Narrow Pores: Phase Equilibria and Structure. *J. Phys.: Condens. Matter.* **1990**, *2*, 8989−9007.
(64) Cole, M. W.; Saam, W. F. Excitation Spectrum and Thermodynamic Properties of Liquid Films in Cylindrical Pores. *Phys. Rev. Lett.* **1974**, *32*, 985−988.
(65) Evans, R.; Marconi, U. M. B.; Tarazona, P. Fluids in Narrow Pores: Adsorption, Capillary Condensation, and Critical Points. *J. Chem. Phys.* **1986**, *84*, 2376−2399.
(66) Nicolaides, D.; Evans, R. Monte Carlo Study of Phase Transitions in a Confined Lattice Gas. *Phys. Rev. B* **1989**, *39*, 9336−9342.
(67) Peterson, B. K.; Gubbins, K. E.; Heffelfinger, G. S.; Marini Bettolo Marconi, U.; van Swol, F. Lennard-Jones Fluids in Cylindrical Pores: Nonlocal Theory and Computer Simulation. *J. Chem. Phys.* **1988**, *88*, 6487−6500.
(68) Zhao, X. S.; Lu, G. Q. Modification of MCM-41 by Surface Silylation with Trimethylchlorosilane and Adsorption Study. *J. Phys. Chem. B* **1998**, *102*, 1556−1561.
(69) Kocherbitov, V.; Alfredsson, V. Assessment of Porosities of SBA-15 and MCM-41 Using Water Sorption Calorimetry. *Langmuir* **2011**, *27*, 3889−3897.

(70) Ng, E.-P.; Mintova, S. Nanoporous Materials with Enhanced Hydrophilicity and High Water Sorption Capacity. *Microporous Mesoporous Mater.* **2008**, *114*, 1−26.
(71) Lamb, R. N.; Furlong, D. N. Controlled Wettability of Quartz Surfaces. *J. Chem. Soc., Faraday Trans. 1* **1982**, *78*, 61−73.
(72) Puibasset, J.; Kierlik, E.; Tarjus, G. Influence of Reservoir Size on the Adsorption Path in an Ideal Pore. *J. Chem. Phys.* **2009**, *131*, 124123−124132.
(73) Kierlik, E.; Puibasset, J.; Tarjus, G. Effect of the Reservoir Size on Gas Adsorption in Inhomogeneous Porous Media. *J. Phys.: Condens. Matter* **2009**, *21*, 155102−155117.
(74) Men, Y.; Yan, Q.; Jiang, G.; Zhang, X.; Wang, W. Nucleation and Hysteresis of Vapor-Liquid Phase Transitions in Confined Spaces: Effects of Fluid-Wall Interaction. *Phys. Rev. E* **2009**, *79*, 51602−51613.
(75) Nguyen, T. X.; Bhatia, S. K. How Water Adsorbs in Hydrophobic Nanospaces. *J. Phys. Chem. C* **2011**, *115*, 16606−16612.